Proceedings of TMCE 2020, 11-15 May, 2020, Dublin, Ireland, edited by I.Horváth and G.Keenaghan

PRELIMINARY STUDY ON END-EFFECTOR COMPLIANCE IN AUTOMATED FLUID COUPLING FOR TRAINS

Kourosh Eshraghi
Department of Mechanical and Aerospace Engineering
Brunel University London
Kourosh.Eshraghi@Brunel.ac.uk

Pingfei Jiang
Department of Mechanical and Aerospace Engineering
Brunel University London
Pingfei.Jiang@Brunel.ac.uk

Daniele Suraci
Department of Mechanical and Aerospace Engineering
Brunel University London
d.t.suraci@gmail.com>

Mark Atherton
Department of Mechanical and Aerospace Engineering
Brunel University London
Mark.Atherton@Brunel.ac.uk

ABSTRACT

In order to improve train availability and workplace safety standards, the rail industry is keen to modernise maintenance of trains through increased use of Robotic Autonomous Systems (RAS). Our research aims to address the mechanical challenges of automated fluid coupling in future applications of train-fluid servicing. Depending on the intricacy of the servicing RAS, a degree of misalignment will always exist between the robot end-effector and train fluid ports. Compliant end-effectors can generate flexing motions that facilitate misaligned insertions. Present work focuses on understanding the role of passive compliance within the end-effector of our demonstrator train fluid servicing robot. Physical experiments were performed and using Design of Experiments we identify the effect of end-effector compliance parameters on misaligned insertions. Results show that maximum insertion force and work done increase exponentially with increasing misalignment. Certain arrangements of compliance parameters can significantly improve the coupling performance under misalignments. Nonetheless, forces observed are still too large and our research will continue to develop compliant end-effectors for better automated coupling that will reduce RAS force requirements.

KEYWORDS

Compliant end-effector, passive compliance, design of experiments, automated fluid coupling, train maintenance

1. INTRODUCTION

1.1. Rail expansion and potential for service automation

It is well documented that UK rail traffic will considerably increase by 2047, requiring a commensurate increase in national passenger fleet of between 5,500 and 12,000 vehicles [1]. This increase will produce a comparative challenge for maintenance depots in terms of increasing their service capacity to keep trains available and reliable. There will also be an increasing demand for accurate service data and asset condition monitoring, vital for modernising maintenance, which will be challenging for manual-based servicing. Not only capacity limits of current manual labour will be stretched, but also the desirability of subjecting humans to such tasks in the 21st century will continue to be scrutinised in terms of working conditions and safety aspects.

It is generally accepted that autonomous servicing could make a positive contribution to meeting the above demands as supported by, for example, an economic and technical feasibility study of a robotic

autonomous system for train fluid servicing [2]. However, it will be technically challenging for an autonomous system to match manual-based servicing in achieving effective mechanical connections common to many train maintenance tasks that are performed under uncertain conditions. Meanwhile, robotic inspection and evaluation of unfamiliar conditions or damage is another challenge.

We have built a research demonstrator robot in order to physically investigate the servicing of train fluids and to specifically focus on the end-effector design for effective and reliable mechanical connection of fluid couplings. This initial "CyberFluids" system (see Figure 1) includes the servicing of fuel, Controlled Emissions Toilets (CET) and wheel sand as pragmatic examples, which has been well received at a demonstration event to the rail industry in March 2019 [3]. Treating this fluid coupling application as akin to a robot assembly task opens up the work to a large body of research in which robot compliance is key to successful robotic manipulations [4].

1.2. Robot compliance

In robotics, compliance (the inverse of stiffness) is defined as the relationship between the motion and forces generated by a robot manipulator and an assembled part at their point of contact. Compliance can commonly be in the form of a spring-like stiffness, a generalised damper or a mechanical impedance. Active compliance is achieved by controlling robot actuators and servo-motions. Passive compliance is defined as intrinsic structural deflections such as flexibility of the robot base, limbs, joint transmissions and compliant end-effector [5]. Active compliance reduces reliance on physical elements and corresponding complexity and also aims at ensuring safety for humans. However, it also presents disadvantages such as power losses, relatively slow dynamic responses and reliance on sensors and control systems. Therefore, passive compliance remains an important feature of most robotic systems and a logical consideration for any new application before active compliance is developed on top.

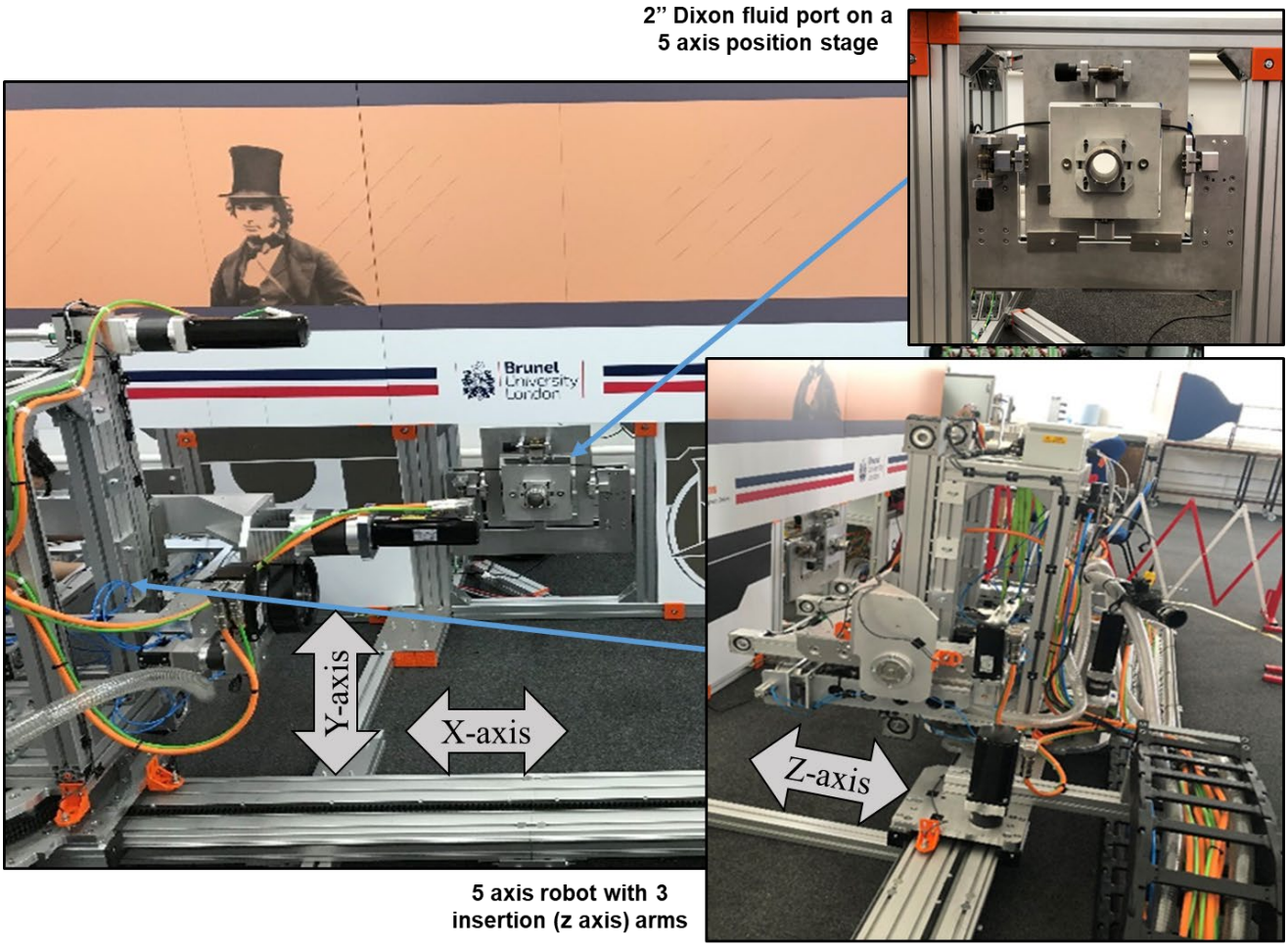

Figure 1 CyberFluids train fluid servicing robot

Compliance of the end-effector is the primary concern in robotic assembly/disassembly where the total positioning tolerance is greater than the assembling tolerance for a 'peg-in-hole' insertion [6]. In such cases, the aim is to avoid wedging or jamming of parts through employing compliance at the end-effector so that motion due to misalignment forces are accommodated. In some peg-in-hole assembly applications, a Remote Centre Compliance (RCC) [7] device projects the compliance centre to a desirable location below or at the point of contact between the assembled parts. An RCC-equipped assembly gripper will pivot the inserting part in a direction that improves alignment as parts contact during the insertion. A Variable Remote Centre Compliance (VRCC) device adapts to various peg lengths by adjusting its RCC projection point [8]. Hence, a single device can proficiently insert various pegs. The idea of RCC is well established and there are other applications such as minimally intrusive surgery. A recent study [9] investigated the design and analysis of a passive RCC device using physical and nonlinear finite element experiments. A projection accuracy of +/- 0.015 mm was achieved for primary stage motions of around +/- 4mm.

Active insertion systems, based on force control algorithms, mimic an ideal RCC mechanism but more recent developments include machine learning, a mixture of sensors and vision systems [10] to solve the peg-in-hole issue. Although the literature is rich, there seems to be a lack of studies that investigate large motion passive devices for the peg-in-hole insertion. Most, if not all, designs incorporate RCC and the inherent principle of instantaneous centre of motion to project the compliance centre. This concept remains valid where motions are small and hence, it is only sufficient for precision assembly applications. For robots outside of controlled environments, e.g. train maintenance, the challenge is to accommodate larger positional uncertainties that accumulate in unstructured environments. In technical terms, a compliant design is considered optimal if the insertion forces for the misalignment range is minimal. This is a motivation for us to investigate compliant end-effectors for our CyberFluids train servicing robot. Providing passive compliance in the mechanical connection of fluid couplings is a type of peg-in-hole scenario.

In this paper, the effect of end-effector compliance on coupling performance is investigated through physical experiments and a resulting second-order regression model. In section 2, we present the end-effector and briefly analyse its performance using Design of Experiments (DoE) where misalignments constitute the uncontrollable factors. Misalignments are representative of practical and inevitable conditions of train position error or robot positional inaccuracy that will be common in future applications of RAS to train servicing. These initial experimental results are presented in section 3 and will serve as a basis for future comparison of end-effectors to be developed. In section 4 the results are discussed, and some recommendations are given to conclude the work in section 5.

2. METHODOLOGY

2.1. CyberFluids' end-effectors

CyberFluids is a Cartesian, track-based robot that runs along an almost full-scale mock-up train carriage that has 2 fluid ports for investigating autonomous servicing. The track alongside the train carriage shown in Figure 1 is the robot X-axis. The robot has 7 Degrees of Freedom (DoF) and provides 5-axis positioning for 3 end-effectors mounted on insertion arms (Z-axis). Two of the Z-axis arms accommodate fluid couplers and the third is for gripping the relevant dust caps. The nominal size of each train port (and cap) corresponds to the typical 2-inch fuel port and 3-inch CET port. The cap gripper has an adjustable jaw to accommodate both cap sizes. On the train side, the 2-inch port is fixed to a manual 5-axis, non-back-drivable, positioning stage that can be used to deterministically misalign the ports.

In current (manual) train fluid servicing operations, many different types of fluid couplers are used to completely service the train. For each type of port coupler different combinations of linear and rotary motions are required to make the coupling. Therefore there is a need to adapt and standardise train fluid ports for automated fluid servicing. Dixon Ez-link cam and groove couplers were selected for this purpose, they only require a linear insertion motion to reliably make a secure and sealed connection. This linear motion will also be less demanding of the robot and end-effector, while making the automated fluid servicing faster. The Cyberfluids end-effector was designed to accommodate the Dixon coupler and actuate its cam-locks. The 2-inch and 3-inch end-effectors are identical in design with 2 pneumatic actuators and a compliant interface with the robot arm. We have selected the 2-inch version for this study. In this section, the end-effector design is evaluated in order to identify design parameters for the DoE.

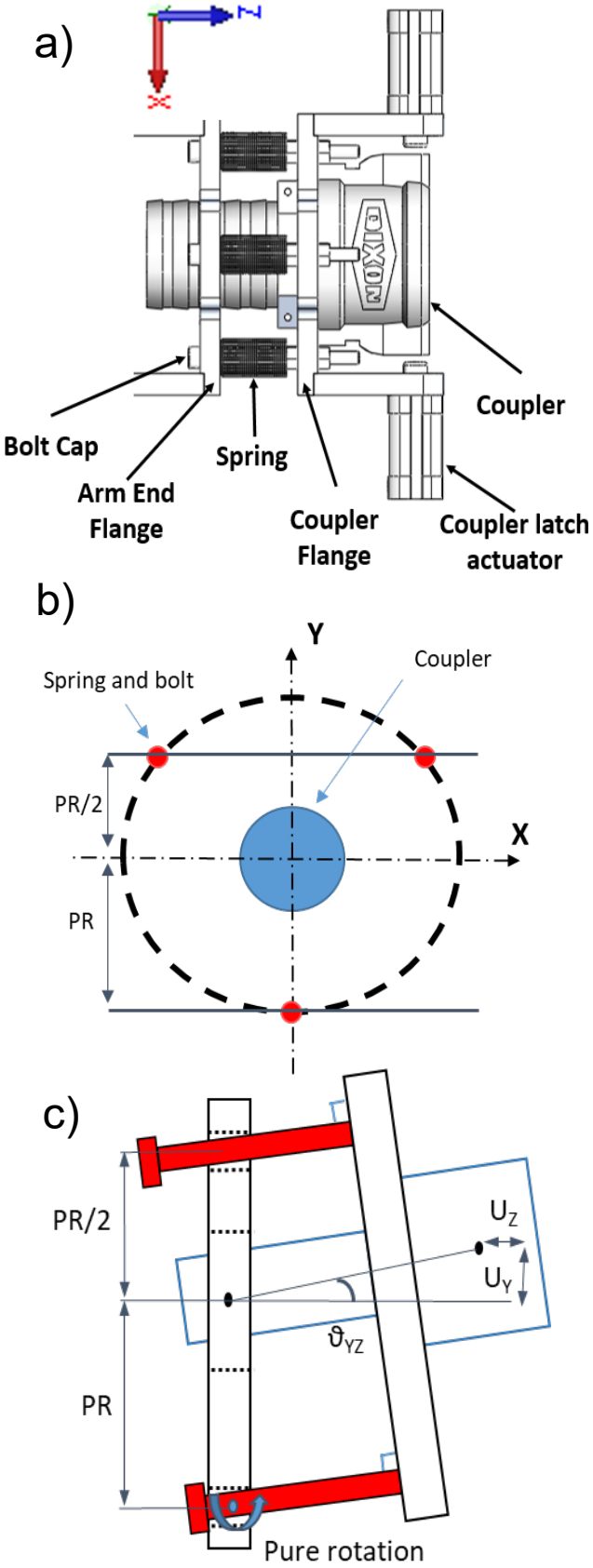

Figure 2 Arrangement of CyberFluids end-effectors

The end-effector has passive compliance facilitated by spring elements, as depicted in Figure 2. It has 3 shoulder bolts encapsulated by springs, the threaded part of the bolt is fixed to the coupler flange while the bolts are free to pivot and slide within corresponding clearance holes located in the arm flange. In this arrangement when all bolts slide simultaneously the motion is linear in the Z direction. The clearance holes effectively act as spherical joints that have corresponding angular motions, which are amplified along the bolt length. The bolts are equally spaced around a pitch circle (radius, *PR*) that coincides with the centre of the coupler. Spring pre-compression ensures that the end-effector returns to its original position after a misaligned insertion. Maximum linear sliding in Z is determined by the compressed length of the springs. The coupler and its flange rotate and slide relative to the arm flange. The maximum rotation occurs when the bolts have two-point contact in the hole. Based on simple geometry a non-linear equation, Equation (1), can be used to estimate this maximum angle.

$$b\sin(\vartheta) + l\cos(\vartheta) = t \qquad (1)$$

Where b is hole diameter, l is hole length and t is bolt diameter and θ is the maximum angle of rotation.

The coupler has 3 DoF (θ_{YZ}, θ_{XZ} and Z). As shown in Figure 2, the X and Y linear motions of the coupler are coupled to the rotations in yaw (θ_{XZ}) and pitch (θ_{YZ}). Hole clearance can encourage small, non-elastic motions in the remaining directions (X Y and θ_{XY}) however, keeping the clearance to a minimum, these motions can be neglected as relatively small. The maximum range of linear motion is not symmetrical either side of the X-axis i.e. in pitch motions. This is because bolts and springs either side of the X-axis have different distances to the coupler centre, as shown in Figure 2a and b. This means that when the plate pivots the amplification effect will be different depending on the direction of motion. For similar reasons, compliance in the pitch axis is also not symmetrical.

2.2. Controllable factors: compliance

We are interested in understanding the effects of spring stiffness, *K*, pitch radius of the bolt holes, *PR* and the orientation of the set of holes, *O*. As discussed in the previous section, clearance will remain a constant and bolt length is not considered (or distance between the arm and coupler flanges) in order to reduce the number of variables (and experiments). Table 1 lists the experimental parameters and Figure 3

Table 1 Experimental parameters

Parameters	Nomenclature	Nominal Value	Experimental Range	Units
Spring Eq. Stiffness	K	4.6	3.2 to 6	N/mm
Pitch Radius	PR	91.5	65 to 118	mm
Bore Orientation	O	0	-25 to +25	°
Bolt Length	L	110	Constant	mm
Bore Clearance	C	0.5	Constant	mm
Coupler/port Clearance	CC	0.7	Constant	mm
X-axis Misalignment	XM	≈0	-5 to 5	mm
Y axis Misalignment	YM	≈0	-5 to 5	mm

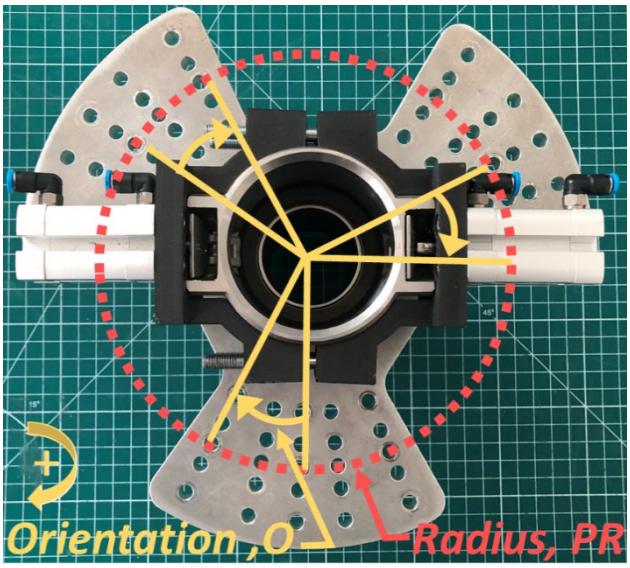

Figure 3 Experimental end-effector

shows the modified experimental end-effector that can accommodate up to 5 adjustable levels for hole orientation, *O*, and pitch radius, *PR*. In order to easily adjust the spring stiffness, *K*, it was decided to use Belleville spring washers (see Figure 4). A number of these spring washers can be stacked in parallel or series to achieve a large range of stiffness, deformation or load characteristics [11]. The selection of Bellville springs is not only constrained by the required range of stiffness or deformation, but also by bolt diameter. If the clearance between the washer and bolt is too large, even when the spring is compressed, washers can slide in the radial direction. This is undesirable as washers will not make contact at consistent points and this will cause an indeterminate change in spring parameters that will induce experimental error. It is also crucial to prevent the

Spring Parameter	Value (mm)
H	0.8
h	0.45
t	0.35
O.D	12.5
I.D	6.2

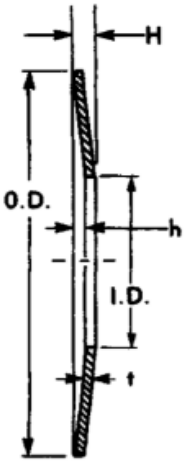

Figure 4 Parameters of the selected Belleville spring washer [8]

washers from jamming in the screw thread. Thus bolt length, *L*, is selected to accommodate the longest spring washer stack. For spring arrangements with a lower free length, standard spacer washers are included in the stack to fill the remainder of the bolt length. All springs arrangements are pre-compressed to 15% of the total stack deformation (lower bound spring operating range recommended in DIN2093). As shown in Figure 5, the selected spring has a nonlinear force-displacement relationship, thus:

$$\frac{df}{dx} \neq Constant\ K \qquad (2)$$

In order to derive a single parameter that serves as the stiffness constant (design parameter, *K*), the force-displacement relationship shown in Figure 5 is linearised. Since the relationship between the number of washers and deformation/load is linear, the regression fit is independent of the number of washers stacked. With R^2=0.898 and *P-Value*= 0.00404, the

regression model has a good fit. Hence linearisation is a simple and reliable method of comparing the stiffness of various washer stack arrangements. Equation 3 is used to identify the number of washers (in series) that will deliver the required linear stiffness.

$$N_{series} = \left(\frac{Linear\ Stiffness\ of\ 1\ washer}{Required\ Linear\ Stiffness}\right)^{Integer} \quad (3)$$

The number of washers must obviously be a discrete value and thus, due to rounding up/down, there are errors in achieving the exact required linear stiffness. However, if a large number of washers are stacked in series this error becomes very small. Using the selected spring, for a range of 3.2 to 6 N/mm (91 to 49 spring washers) maximum error in the stiffness is 0.064%

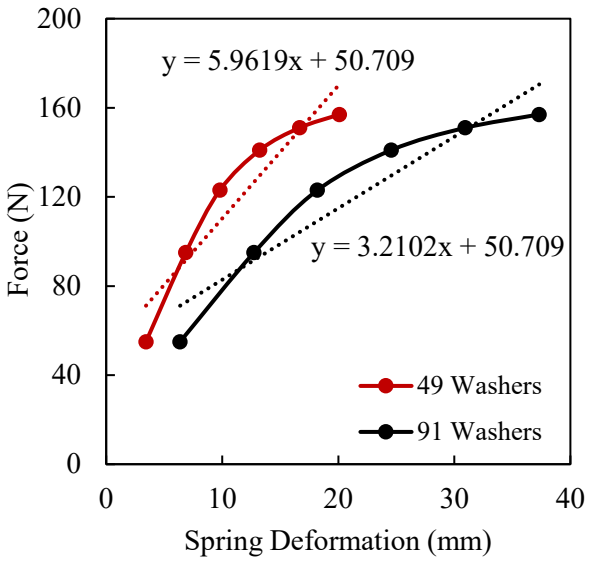

Figure 3 Force displacement relationship of the selected Belleville washers

2.3. Noise factors: misalignments

For an XYZ (3 DoF) Cartesian RAS conceptualised in [2], robot X and Y-axis misalignments lead to poor coupling. Axial misalignments in Z (insertion direction) only contribute to the coupling seal hence neglected in present work. For these experiments train fluid ports are aligned parallel to the robot Z-axis and the CyberFluids robots will only use XYZ motion to make the fit. Initial experiments determined that ports do not couple when X and Y axes are misaligned more than 5 mm. Hence, the experimental range of misalignments is selected accordingly. Misalignments are measured using Vernier callipers from a fixed datum on the fluid port positioning stage.

2.4. Performance measurement: readings

A perfectly aligned fluid coupling is expected to couple with minimal force; a high insertion force will indicate high friction and/or physical clash that will occur due to misalignment between the coupler and fluid port. Therefore, considering the complete insertion cycle, we can use the energy quantity, work done by the motor, as a scalar measure of coupling performance. Insertion force is also monitored, as this is important for sizing actuators, robot structure and preventing damage to the robot or train parts.

Robot servo-drives can monitor motor current and position, which is used to determine insertion force and linear position of the end-effector arm. The relationship between motor current and torque is linear and defined by a motor torque constant specified by the manufacturer. In order to obtain work done, torque must be converted to force and integrated over the linear distance travelled.

$$\text{Motor Torque}, T_M = k_M * I_{rms} \quad (4)$$

$$\text{earbox }, T_G = T_M * 5 \quad (5)$$

$$\text{Insertion Force}, F_z = T_G/r \quad (6)$$

$$\text{Work}, W = \int F_z d_Z \quad (7)$$

Where k_M is the motor torque constant, Irms is the root mean square of the 'torque generating' current and r is the radius of the pulley drive in the insertion arm.

The servo-drive is capable of recording 200 samples for motor position and current. The robot insertion speed was set to a nominal value of 25mm/s, and a sampling rate of 20ms was used in order to capture the entire event of coupling with sufficient precision.

2.5. Design of Experiments (DoE)

A DoE [12] approach was employed in order to maximise the chances of meaningful experimental results. DoE methods introduced in many textbooks place emphasis on factors with two levels, often called 2k-p design, where k is the number of factors and p is the degree of fractionation. DoE methods such as full factorial and fractional factorial design are widely applied in 2-level factor DoE. Despite the advantages of having only 2-level factors such as reduced experiment size and simple analysis of main effects and interactions [13], it is inadequate for predicting precise and non-linear behaviour of the system output due to factor changes. Response surface methodology (RSM) can be seen as a branch of DoE with the

purpose of fitting regression models and optimising processes and systems [14]. Central Composite Design (CCD) was adopted in this study due to its wide application [14]. When allocating design points three types of CCD can be applied, namely circumscribed (CCCD), inscribed (ICCD) and faced (FCCD). CCCD tends to create new extreme limits for factors, indicated by the four axial points outside design space. ICCD can be seen as a scaled-down version of CCCD with axial points created inside the design space. For CCCD larger factor limits are physically impossible to achieve with the current design. For ICCD no combination of factors at extreme levels are investigated, e.g. largest misalignments in X and Y at the same time. Therefore FCCD was adopted in this study which investigates the influence of robot end-effector design factors on the resultant energy consumption to perform an effective coupling. An FCCD for five factors of *K*, *PR*, *O*, *XM* and *YM* requires 36 experiments with each factor at 3 levels, including the extremes and midpoints of the experimental range (see Table 1). Typically, system responses are represented by regression functions with appropriate empirical models that allow prediction with known factors. These regression functions can exist in various formats such as first-order or second-order polynomial models, describing linear and quadratic behaviour of system responses respectively. Equation 8 is a general expression of a second-order regression model.

$$R = \beta_0 + \sum_{i=1}^{n} \beta_i x_i + \sum_{i=1}^{n} \beta_{ii} x_i^2 + \sum_{i=1}^{k} \sum_{j=2}^{n} \beta_{ij}\, x_i x_j + \varepsilon$$

R represents system response, n stands for the number of factors, x_i stands for each independent factor, β are the coefficients for each independent term and $\boldsymbol{\varepsilon}$ is the error term.

For a complex device like the robot end-effector design studied here, a second-order regression model is chosen as non-linear behaviour of its response upon factor changes is expected. Each factor in an FCCD is configured to three levels: low, medium and high. These levels are generally codified as -1, 0 and 1 respectively. Actual settings for each factor were then interpolated referring to their actual limits. Table 2 shows the experimental plan in actual values using FCCD with a revised order to minimise human effort in changing end-effector configurations. Furthermore, centre runs were performed at different points during the experiments in order to effectively capture more of experimental errors.

Table 1 Faced Central Composite Design of Experiments plan with the obtained results

Order	K	PR	O	XM	YM	Work (Nm)	Max Force (N)	Order	K	PR	O	XM	YM	Work (Nm)	Max Force (N)
1	4.6	91.5	0	0	0	1.89	49.64	**19**	6	65	-25	-5	-5	4.20	329.85
2	4.6	91.5	0	0	0	2.03	60.85	**20**	6	65	-25	5	5	6.05	521.99
3	4.6	91.5	0	0	0	1.94	59.24	**21**	6	65	25	-5	5	8.92	611.66
4	4.6	91.5	0	0	0	1.89	51.24	**22**	6	65	25	5	-5	3.42	209.76
5	4.6	91.5	0	0	0	1.89	49.64	**23**	3.2	65	25	-5	-5	3.73	285.01
6	4.6	91.5	0	-5	0	4.92	414.71	**24**	3.2	65	25	5	5	7.46	542.81
7	4.6	91.5	0	0	0	1.98	60.85	**25**	3.2	118	-25	-5	-5	4.30	344.26
8	4.6	91.5	0	0	0	1.89	48.04	**26**	3.2	118	-25	5	5	10.78	643.68
9	4.6	91.5	0	5	0	3.04	163.32	**27**	6	118	-25	-5	5	11.13	648.49
10	4.6	91.5	0	0	-5	2.66	118.49	**28**	6	118	-25	5	-5	3.86	291.42
11	4.6	91.5	0	0	5	5.67	493.17	**29**	6	118	25	-5	-5	9.34	630.87
12	3.2	91.5	0	0	0	2.04	60.85	**30**	6	118	25	5	5	9.03	650.09
13	6	91.5	0	0	0	2.06	67.25	**31**	3.2	118	25	-5	5	9.30	570.03
14	4.6	91.5	-25	0	0	2.01	60.85	**32**	3.2	118	25	5	-5	3.68	257.79
15	4.6	91.5	25	0	0	2.17	76.86	**33**	4.6	118	0	0	0	2.06	68.85
16	4.6	65	0	0	0	2.08	73.66	**34**	4.6	91.5	0	0	0	2.09	73.66
17	3.2	65	-25	-5	5	9.32	611.66	**35**	4.6	91.5	0	0	0	1.96	59.24
18	3.2	65	-25	5	-5	3.41	261.00	**36**	4.6	91.5	0	0	0	1.95	57.64

3. RESULTS

Table 2 shows the results that were post-processed according to the formulations of Section 2.4. The trapezium rule of integration was employed to numerically calculate the work done. Two independent regression models were developed based on work done and maximum insertion force (Max-Force). The model fit statistics are listed in Table 3. Both models are significant (*P-value* < 0.05) and express very good prediction capability with R^2 values close to 1. Table 4 shows the regression coefficients and P-values that represent the significance of each term in the regression model. The main and quadratic effects of misalignments are very sizeable. Spring stiffness, *K,* and pitch radius, *PR,* are effective design parameters while hole set orientation, *O,* is not. The quadratic effect of design factors are insignificant however, most interaction terms, especially those involving *K*, are significant.

Figure 6 is a typical experimental reading in which it is possible to see the force-displacement relationship of the robot arm. Typically, 45 N is required to drive the arm at the set speed of 25 mm/s. Based on the Max-Force prediction model, Figure 7 shows that when both misalignments are large, maximum force could reach up to a value of 660 N.

Figure 8 shows the mean effect of the significant factors in terms of the observed work done. By averaging, the observed responses when each factor was at its higher or lower limits, the typical effect of a design factor is determined [15]. Softer springs and lower values of *PR* results in lower work done. Obviously, coupling with large misalignments should produce a higher value of work done. However, mean response is significantly lower in the $-Y$ and $+X$ directions. This is understandable for the Y-direction as pitch compliances are not symmetrical. It is interesting to have observed this in the X direction as this could indicate systems' (end-effector, robot and fluid port) preferred directions of compliance. This phenomenon and the lack of symmetry are also observable in Figure 7 as the red and blue lines do not overlap.

Figure 9 shows the surface plot based on the work-model. It shows the effects and interactions of *PR* and *K*. When both of these factors are at their lower level, significantly less work done is required to make the coupling.

Plots of Figure 10 are based on the Max-Force prediction model. Again, the quadratic effect is very clear. Design factors *K* and *PR* reduce maximum force significantly. When using the softest springs, the average reduction is 43 N, when pitch radius is minimum this value is 73N, and when both parameters are set to their lowest values, its 115 N with a maximum reduction of 170N when X-axis is misaligned 5mm in the negative direction. It can also be observed that at time Max-Force reaches values below 0. These regression model predictions are not true in physical reality. This is due to the fit of the regression model and in Figure 11 the residuals (difference in real and predicted response) for each observation highlight that some of the experiments have large residuals.

(18)

Table 3 Fit statistics of the regression models

Statistics	'Work' Model	'Max-Force' Model
Error Degrees of Freedom	15	15
Root Mean Square Error	0.429	40.7
R^2	0.991	0.986
Adjusted R^2	0.98	0.968
P-Value	5.91e-12	1.45e-10

Table 4 Coefficients of the regression models

	Work		Max-Force	
	B	P-Value	B	P-Value
(Intercept)	1.932	0.000	67.366	0.000
K	0.221	0.045	21.349	0.042
PR	0.827	0.000	36.561	0.002
O	0.111	0.290	6.761	0.492
XM	-0.801	0.000	-50.260	0.000
YM	2.170	0.000	142.507	0.000
K^2	0.141	0.615	-16.272	0.539
PR^2	0.163	0.560	-9.066	0.731
O^2	0.182	0.516	-11.468	0.664
XM^2	2.072	0.000	208.697	0.000
YM^2	2.254	0.000	225.509	0.000
K.PR	0.414	0.002	27.020	0.018
K.O	0.570	0.000	32.224	0.006
K.XM	-0.619	0.000	-27.621	0.016
K.YM	-0.465	0.001	-15.612	0.146
PR.O	0.048	0.661	16.012	0.136
PR.XM	-0.055	0.613	-3.002	0.772
PR.YM	0.130	0.243	-13.410	0.207
O.XM	-0.178	0.118	-13.810	0.195
O.YM	-0.435	0.001	-13.010	0.220
XM.YM	0.116	0.299	30.423	0.009

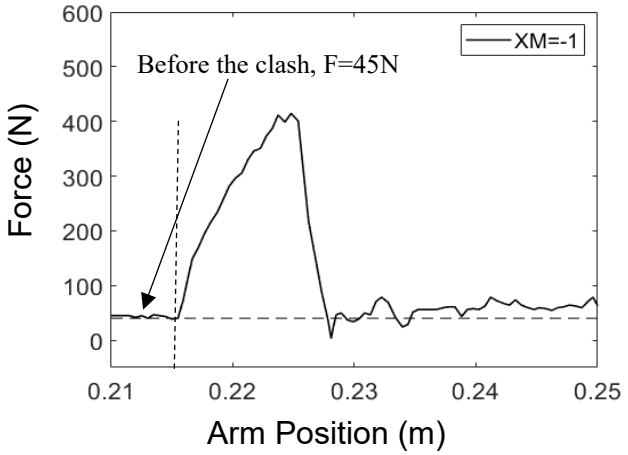

Figure 6 Experimental Force-Position curve for misaligned insertion

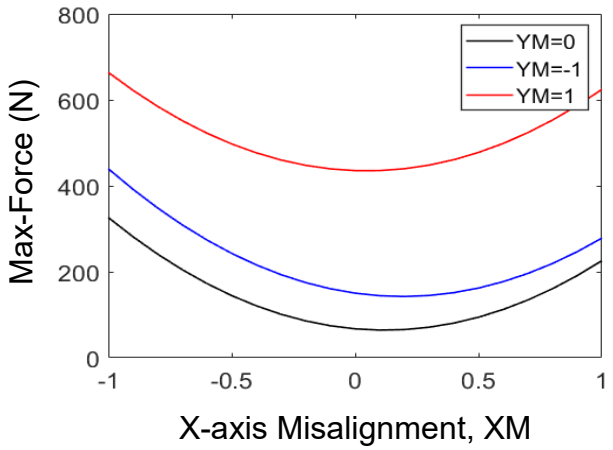

Figure 7 Prediction of Max Force at nominal design condition and varying misalignments

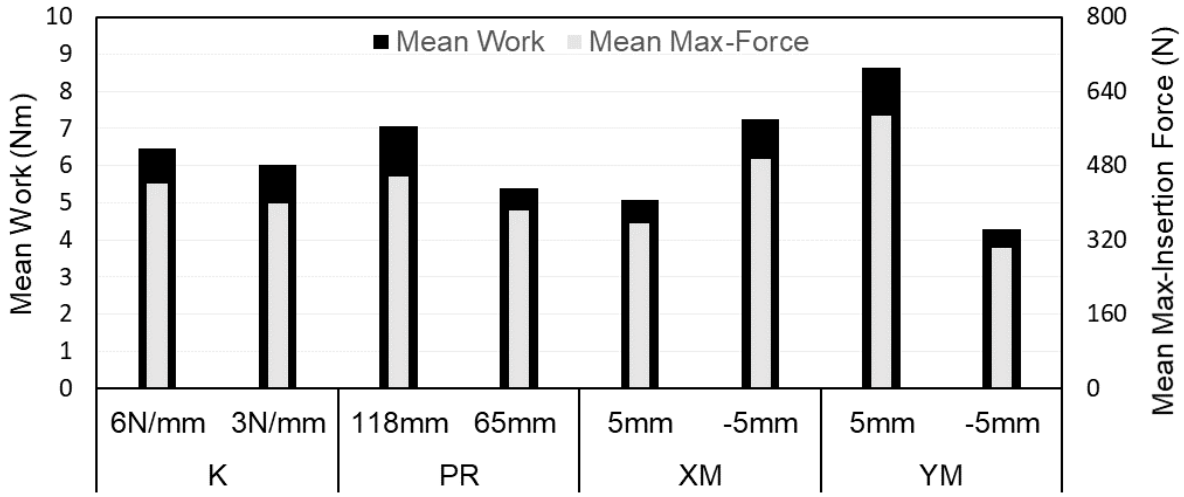

Figure 8 Mean effect of experiment factors based on physical data

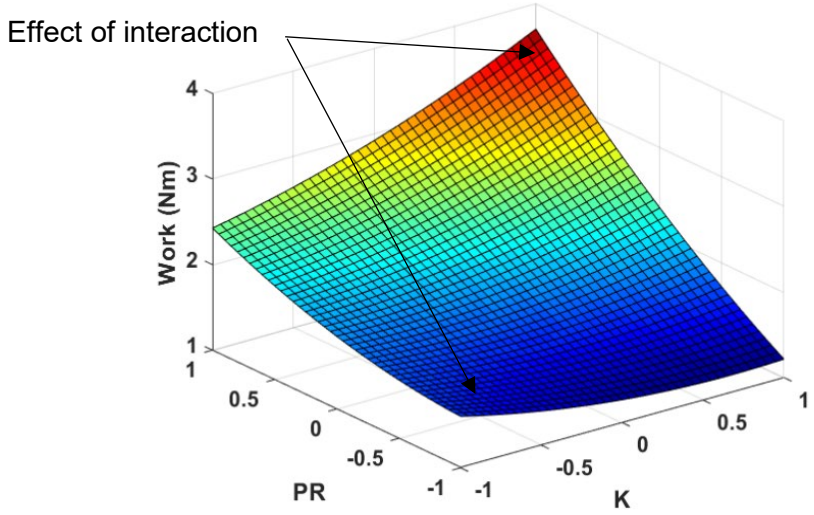

Figure 9 Predicted response surface plot: showing the interaction of design factors

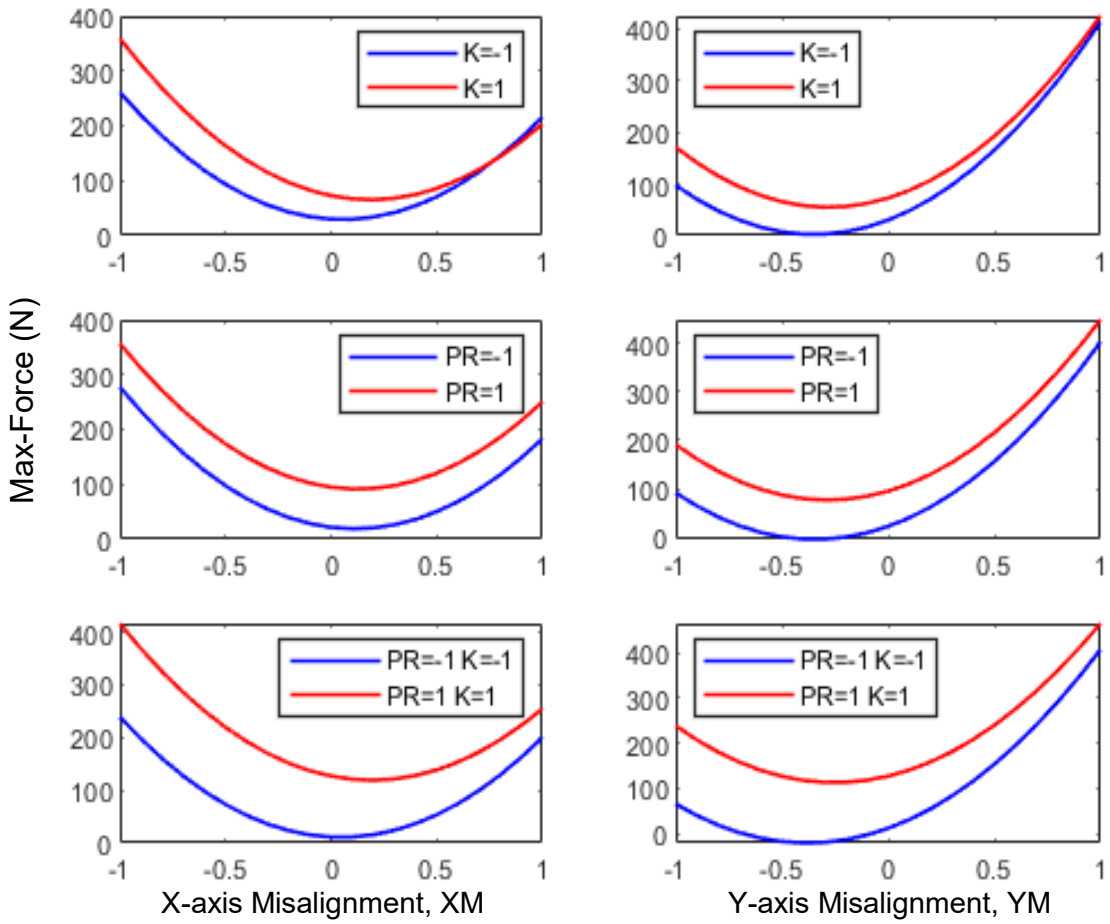

Figure 10 Prediction of maximum insertion force with varying misalignment conditions: showing the effect of design factors on Maximum insertion Force

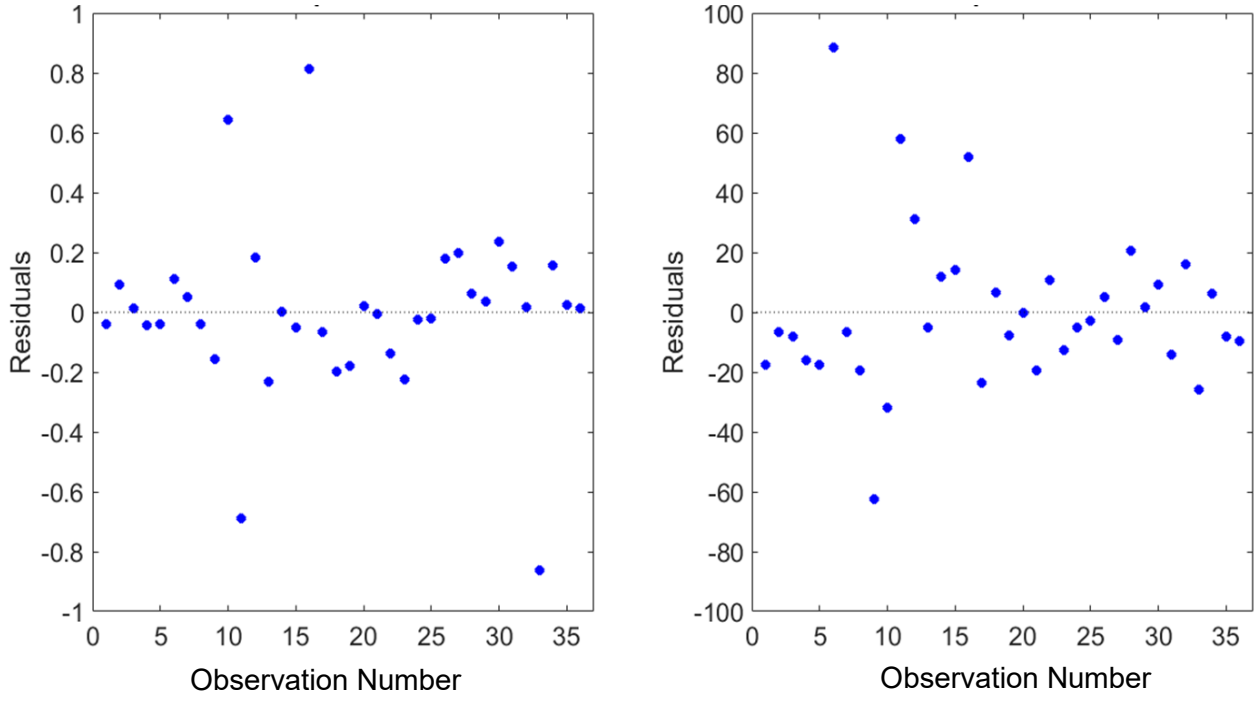

Figure 11 Plots of error in real and estimated responses (plot of residuals)

4. DISCUSSION

Compliances of the end-effector are not symmetrical in pitch motions. When the coupler pivots downwards it only deforms one spring, if it pivots upwards it will press on two springs. Thus pivoting downwards due to a corresponding misalignment requires less work or force. This has encouraged a lack of symmetry in the results which is also augmented by experimental error, robot inherent compliance, backlash and other hysteresis that creates preferred directions of motion. Robot compliances could overshadow the end-effector compliance and explain the relatively lower mean effect of design parameters. For future experiments, where only end-effector compliance is of interest, fixing and rigidising all but the insertion axis of the robot will be beneficial in isolating the effects of the end-effector compliance. Nevertheless testing the end-effector 'in-situ' is important for representing the real application.

It can also be observed that the second order regression model has limited ability to capture the actual non-linearity. Although the regression statistics suggest a very good fit, when the work done or forces are low the predicted response can go negative in cases of Y-misalignments. This could have been triggered by the lack of symmetry in the end-effector compliance however, increasing the number of experimental levels to 5 could considerably improve this issue.

Overall results show that generally more compliant springs reduce the work done. We also observed an interaction between pitch radius and spring stiffness. When both are at their lowest values, a significant increase in performance is observed. This is intuitive in that moments exerted by the spring are reduced at lower pitch reduces. When there are no misalignments, a force of about 45 N is required to drive the robot arm at the nominal speed. Force observed beyond this value is due to contact friction and physical clash. When the port is misaligned 5mm in X and Y, the maximum insertion force is around 660N. This value is very large when compared to the typical force exerted manually by a human. Train fluid ports are not designed for such loads, which also increases requirements on the robot such that larger motors and structures become necessary.

As understood from a typical peg-in-hole problem, when the misaligned peg travels across the chamfer and is inserted, angular motions of the peg could result in 2-point contacts that encourage jamming. The current end-effector only moves in pitch, yaw and the insertion directions and thus coupling is often prone to jamming as misalignments are linear. The Cyberfluids robot is capable of generating large forces that exceed the jamming force. The robot arm then bounces forwards and the springs release energy, hence the sudden drop of force in Figure 6.

Simple modifications to the CyberFluids end-effector can increase its performance and help to prevent reduce insertion forces. By incorporating clearance holes in the coupler flange, and removing the locking nuts from the spring side, the coupler will attain pivoting capabilities relative to the bolt. In 2D, this arrangement becomes analogous to a parallelogram linkage. The double pivoting action stacks to allow linear motion in X or Y. It also desirable to have symmetrical compliance in the X-Y plane, thus 4 equally spaced springs should be incorporated. 2 along the Y-axis and 2 along the X-axis. Compliance in the insertion direction is not necessary but it is inherent to this end-effector design concept. Nonetheless, this feature could be useful as a safety feature for robots that cannot limit force/torque of actuators.

Flexure mechanisms [16] have become very popular over the last two decades. There are many inherent advantages in solving the same design problem using monolithic, distributed compliance mechanisms. Good examples are Constant Force Mechanisms (CFM) [17] that regulate surface contact forces and generate compliance at the end-effector. Therefore, in developing new compliant end-effectors, flexure-based mechanism incorporating passive compliance capable of handling a larger range of misalignments will be developed for a peg-in-hole scenario. Such an end-effector can solve another limitation of our work; where we assumed ports would be horizontally located on the train. Depending on how the rail industry goes forward with modifying the fluid ports, simple robots with compliant end-effectors could deliver a better economic solution than to very sophisticated robots with many sensors and DoF.

5. CONCLUSION

Automated servicing of trains is being seriously considered by the rail industry with the aim of releasing humans from unsuitable tasks and improving health and safety in maintenance depots. The benefit of having passive compliance in a robot end-effector will help to improve the robustness of fluid coupling whilst reducing the reliance on accurate robot end-effector positioning systems. In this work, we have investigated the role of end-effector compliance in

enhancing the mechanical connection of fluid ports under positional uncertainties. Results show that misalignments have an exponential effect on the work done and the maximum force of insertion. When the fluid port is misaligned, having softer springs at a lower pitch radius can reduce the maximum insertion force by up to 160N. Likewise, work done by the end-effector is reduced indicating a better coupling. Yet still the forces involved are too large and need to be reduced. As discussed, small modifications to the current end-effector design can result in better coupling performance. This is a next step in our research on end-effector compliance design, which focuses on relaxing the insertion force relationship to misalignments.

Through this preliminary study, it is apparent that a Design of Experiments with more levels will increase the accuracy of the prediction model. In addition, the inherent robot compliances and hysteresis can enhance or disturb the coupling process. Hence, future experiments will use a highly rigid rig for isolating end-effector compliance more effectively.

ACKNOWLEDGEMENTS

We especially thank and acknowledge the Rail Safety and Standards Board (RSSB) for funding and supporting this research (contract RSSB 2675).

REFERENCES

1. Eversholt Rail Group; Angel Trains; Porterbrook; Rail Delivery Group. Long term passenger rolling stock strategy for the rail industry. 6th ed., Rail Delivery Group, 2018.
2. Atherton, M.; Hill, S.; Harrison, D.; Ajovalasit, M. Economic and technical feasibility of a robotic autonomous system for train fluid servicing. J. Rail Rapid Transit, 2019.
3. Rail Safety and Standards Board, Fluid servicing robot – developed by Brunel University with TBG Solutions, 2019 https://www.youtube.com/watch?v=cMn5AIZbx0U&t=4s accessed 5 November 2019.
4. Ang, M.H. and Andeen, G.B., 1995. Specifying and achieving passive compliance based on manipulator structure. IEEE transactions on robotics and automation, 11(4), pp.504-515.
5. Wang, W., Loh, R.N. and Gu, E.Y., 1998. Passive compliance versus active compliance in robot-based automated assembly systems. Industrial Robot: An International Journal, 25(1), pp.48-57.
6. Zhang, Y., Lu, H., Pham, D.T., Wang, Y., Qu, M., Lim, J. and Su, S., 2019. Peg–hole disassembly using active compliance. Royal Society open science, 6(8), p.190476.
7. Whitney, D.E., 1979. What is the remote centre compliance (RCC) and what can it do?. In Proceedings of the 9th International Symposium on Industrial Robots, 1979.
8. Lee, S. (2005). Development of a New Variable Remote Center Compliance (VRCC) With Modified Elastomer Shear Pad (ESP) for Robot Assembly. *IEEE Transactions on Automation Science and Engineering*, 2(2), pp.193-197.
9. Gandhi, P., Bobade, R. and Chen, C. (2018). On novel compliant mechanisms for remote center motion. *Advances in Mechanical Engineering*, 10(4), p.168781401876192.
10. Xu J, Hou Z, Liu Z, et al. Compare contact model-based control and contact model-free learning: A survey of robotic peg-in-hole assembly strategies. Preprint (2019), arXiv:190405240.
11. Shigley, J. (2006). Standard handbook of machine design. 2nd ed. Norwich, NY: Knovel.
12. Montgomery D. C., Design and analysis of Experiments, 5th ed. USA: John Wiley & Sons, Inc., 2001.
13. Ankenman, B. E. “Design of Experiments with Two- and Four-Level Factors,” J. Qual. Technol., vol. 31, no. 4, pp. 363–375, 1999.
14. Myers R. H., “Response surface methodology - Current status and future directions,” J. Qual. Technol., vol. 31, no. 1, pp. 30–44, 1999.
15. Atherton, M. A. and R. A. Bates, “Searching for improvement,” in Design and Information in Biology, vol. 27, WIT Press, 2006, pp. 345–379.
16. Howell, L., Magleby, S. and Olsen, B. (2013). *Handbook of compliant mechanisms*. Chichester (United Kingdom): John Wiley & Sons.
17. Chen, Y. and Lan, C. (2012). An Adjustable Constant-Force Mechanism for Adaptive End-Effector Operations. *Journal of Mechanical Design*, 134(3).